Front. Electr. Electron. Eng. China 2007, 2(1): 92–98
DOI 10.1007/s11460-007-0017-8

RESEARCH ARTICLE

ZHOU Zhi, LI Jilong, OU Jinping

Interface transferring mechanism and error modification of embedded FBG strain sensors

Abstract As the strain sensing element of a structural health monitoring, the study and the application of the fibre-optic bragg grating (FBG) have been widely accepted. The accuracy of the FBG sensor is highly dependent on the physical and the mechanical properties of the strain interface transferring characteristics among the layers of bare optical fibre, protective coating, adhesive layer and host material. In this paper, firstly, the general expression of the multilayer interface strain transferring mechanism is derived. Secondly, based on the defined average strain, the error-modified equation of the FBG sensor is obtained. Finally, in the light of the embedded tube-packaged FBG and the fibre reinforced polymer-optical fibre bragg grating (FRP-OFBG) strain sensors, developed in the Harbin Institute of Technology (HIT), the corresponding strain transferring laws have been studied, and the corresponding error modification coefficients have also been given, which are validated by experiments. The research results provide theories for the development and application of the embedded FBG sensors.

Keywords FBG, strain sensor, strain interface transferring, error modification

1 Introduction

The structure of the fibre-optic strain sensors commonly includes the fibre-optic, a protective coating and an adhesive layer, but according to the different demands of installation techniques, other encapsulated materials can be added.

The influences to the strain transferring of every layer are different. In a mechanical structure, the biggest difference between the fibre-optic bragg grating (FBG) sensors and the fibre-optic strain sensors is that the former doesn't have protective coating, namely, the FBG is a bare optical fibre. While in application, encapsulations or protections are usually adopted. The material properties and dimension effects of the layers will certainly result in a discrepancy between the respondent strains of the FBG sensors and the practical ones, which are the main source of the system errors in an FBG sensor. The multilayer interface strain transferring mechanism and the error modification are the bases of researching, developing and applying in FBG sensors.

The interface transferring properties of the fibre-optic sensors have already brought correlative scholars to pay attention to this field, and some useful accomplishments have been gained. In 1991, Antonio Nanni [1] roughly gained the relationship between the testing strains of the fibre-optic sensors and the concrete strains, which is expressed as

$$\varepsilon_{\text{optical fibre}} = \varepsilon_{\text{concrete}} \frac{2E_{\text{protective coating}}}{E_{\text{concrete}} + E_{\text{protective coating}}}$$

Although Ansari [2], Duck [3] et al. also presented the corresponding fibre-optic sensing mechanical model, they didn't consider the influence of the adhesive layer thickness and the encapsulated materials. Hence it is difficult to analyze the encapsulation and the installation techniques of the fibre-optic sensors. The fibre-optic sensing model given by Lau et al. [4] ignored the effects of the shape of the host material and the practice applications while the optical fibre is longer though the influence of the adhesive layer was considered. So the problems induced by the protective coating, encapsulation and adhesive could not be well accounted for either. In the field of experiment and theory, there are a lot of works that have been done by some scholars in China [5–8].

This paper aims at the common situation of FBG strain sensing, and focuses on the strain sensing problem of the FBG sensors with protective coating embedded in the structure via an adhesive layer to derive the general expression of the multilayer interface strain transferring mechanism. Besides, based on the defined average strain, the error modified equation of the FBG sensor is obtained. Finally, in light of the embedded tube-packaged FBG and FRP-OFBG strain sensors developed in HIT, the corresponding strain

Translated from *Journal of Harbin Institute of Technology*, 2006, 38(1): 49–55 [译自: 哈尔滨工业大学学报]

ZHOU Zhi (✉), LI Jilong, OU Jinping
School of Civil Engineering, Harbin Institute of Technology, Harbin 150090, China
E-mail: zhouzhi@hit.edu.cn

transferring laws have been studied, and the corresponding error modification coefficients have also been given and validated by experiments.

2 Interface transferring mechanism of an embedded FBG strain sensor

2.1 Cylindrical model and displacement relationship

First, in Figs. 1 and 2, given a rectangular section beam, under the basic sensing mode of a bare optical fibre, protective coating, adhesive layer and a host material, the FBG strain sensing characteristics are analyzed mechanically. The deriving methods of the other form sections are similar.

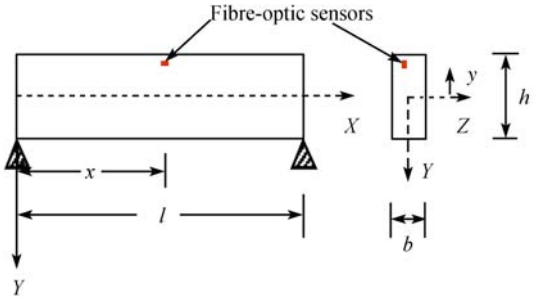

Fig. 1 Rectangular beam with the embedded optical fibre sensor

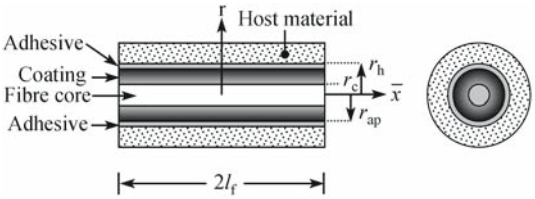

Fig. 2 Cylindrical model of optical fibre strain sensing

Because the optical fibre is embedded in the host material and with the same axial symmetry, the circular cylindrical coordinates are shown in Fig. 2. Thereinto $\bar{x}$ is the axial coordinate and r is the radial coordinate with the symbols r_h, r_{ap}, r_c and b represents the inner radii of the host material, the outer radii of the protective coating and bare fibre, which are respectively measured from the centre of the fibre core; $2l_f$ is the effective working length of the FBG sensors.

We introduce the following basic hypotheses.

1) The optical fibre, proactive coating, adhesive layer and host material are in linear elastic isotropy.

2) All of the adhesive interfaces are continuous and satisfy the displacement compatibility.

3) Without regard to the temperature effect.

According to the hypotheses of displacement continuousness, there is a relative displacement between the optical fibre and the host material, which results from the shear deformations of the protective coating and adhesive layer. In

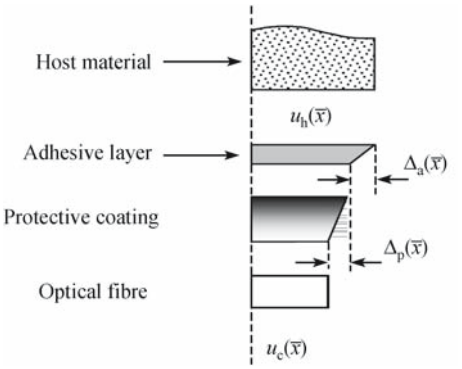

Fig. 3 Relationship of deformation for cylindrical model

Fig. 3 (for the axial symmetry, showing a four-cylinder model), the relative displacements Δ are given by

$$u_h(\bar{x}) = \Delta_a(\bar{x}) + \Delta_p(\bar{x}) + u_c(\bar{x}) \tag{1}$$

$$\Delta_a(\bar{x}) = u_a(r_h, \bar{x}) - u_a(r_{ap}, \bar{x}) \tag{2}$$

$$\Delta_p(\bar{x}) = u_p(r_{ap}, \bar{x}) - u_p(r_c, \bar{x}) \tag{3}$$

where the symbols $u_c(\bar{x})$, $u_p(r, \bar{x})$, $u_a(r, \bar{x})$ and $u_h(\bar{x})$ represent the displacement of the optical fibre, protective coating, adhesive layer and the host material respectively. When $\bar{x} = 0$, the strains for all layers are mathematically identical, i.e.,

$$\varepsilon_h(r,0) = \varepsilon_a(r,0) = \varepsilon_{ap}(r,0) = \varepsilon_c(r,0) \tag{4}$$

2.2 Balance equation for infinitesimal element

1) Balance equation of fibre-optic infinitesimal element

Since the optical fibre is insensitive to the transverse stresses [9], the effects of the transverse normal and shear stresses are therefore ignored, and only the lengthwise normal and shear stresses are considered. By considering the axial forces equilibrium for an element of the optical fibre at arbitrary point $\bar{x}$, shown in Fig. 4, we can obtain an equation simplified as

$$\frac{\mathrm{d}\sigma_c(\bar{x})}{\mathrm{d}\bar{x}} = -\frac{2\tau_{pc}(r_c, \bar{x})}{r_c} \tag{5}$$

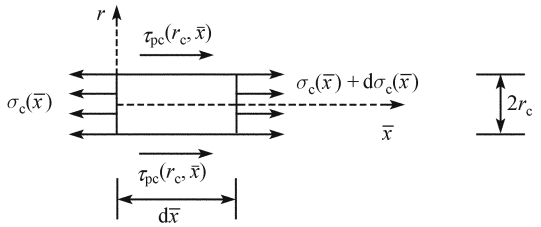

Fig. 4 Infinitesimal element of optical fibre

2) Balance equation for infinitesimal element of protective coating and adhesive layer

Figure 5 is the infinitesimal element of the protective coating. According to the relationship of deformation compatibility, an approximate expression [10] can be obtained by

$$\tau(r,\bar{x})=\frac{r_{ap}}{r}\tau_{ap}\left(r_{ap},x\right),\qquad r_c\leqslant r\leqslant r_{ap} \tag{6}$$

$$\tau(r,\bar{x})=\frac{r_{ap}}{r}\tau_{ap}\left(r_{ap},\bar{x}\right),\qquad r_{ap}\leqslant r\leqslant r_h \tag{7}$$

Considering the $\sum F_{\bar{x}}=0$, we can obtain

$$\frac{\mathrm{d}\sigma_p(\bar{x})}{\mathrm{d}\,\bar{x}}=\frac{2\left[\tau_{pc}\left(r_c,\bar{x}\right)\,r_c-\tau\left(r_{ap},\bar{x}\right)\,r_{ap}\right]}{{r_{ap}}^2-{r_c}^2}$$

When $r=r_c$, by Eq. (6), there is $\tau_{pc}\left(r_c,\bar{x}\right)\,r_c=\tau\left(r_{ap},\bar{x}\right)\,r_{ap}$, then the last equation becomes $\dfrac{\mathrm{d}\sigma_p(\bar{x})}{\mathrm{d}\bar{x}}=0$, namely,

$$\sigma_p(\bar{x})=\text{constant},\ \sigma_a(\bar{x})=\text{constant} \tag{8}$$

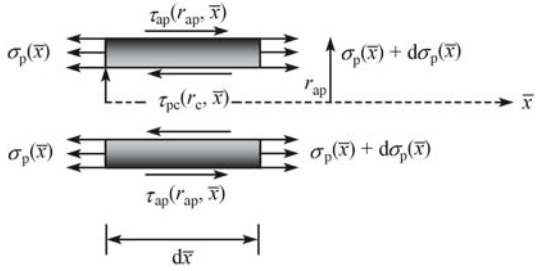

Fig. 5 Infinitesimal element of protective layer

3) Relationship between normal and shear stress at a need testing point of the host material.

If the effective testing length of the optical fibre is less, we can regard

$$\sigma_h(\bar{x})=\text{constant} \tag{9}$$

On the contrary, if the effective testing length of the optical fibre is not less, according to material mechanics, we can realize

$$\frac{\mathrm{d}\sigma_h(\bar{x})}{\mathrm{d}\bar{x}}=\frac{\tau(r_h,\bar{x})\ by}{S_z^*} \tag{10}$$

where S_Z^* represents the geometrical moment of inertia.

4) Balance equations of displacements and stresses

Due to the physics equations, we can learn

$$\begin{cases}\varepsilon_h(\bar{x})=\dfrac{\sigma_h(\bar{x})}{E_h}, & \varepsilon_c(\bar{x})=\dfrac{\sigma_c(\bar{x})}{E_c}\\ \gamma_a(r,\bar{x})=\dfrac{\tau(r,\bar{x})}{G_a}, & r_{ap}\leqslant r\leqslant r_h\\ \gamma_p(r,\bar{x})=\dfrac{\tau(r,\bar{x})}{G_p}, & r_c\leqslant r\leqslant r_{ap}\end{cases} \tag{11}$$

and the axial displacements of the host material and the optical fibre and the relative displacements of the adhesive layer and the protective coating are given by

$$\begin{cases}u_h(\bar{x})=\int_0^{\bar{x}}\varepsilon_h(\bar{x})\ \mathrm{d}\bar{x}=\int_0^{\bar{x}}\dfrac{\sigma_h(\bar{x})}{E_h}\mathrm{d}\bar{x}\\ u_c(\bar{x})=\int_0^{\bar{x}}\varepsilon_c(\bar{x})\ \mathrm{d}\bar{x}=\int_0^{\bar{x}}\dfrac{\sigma_c(\bar{x})}{E_c}\mathrm{d}\bar{x}\end{cases} \tag{12}$$

$$\begin{cases}\Delta_a(\bar{x})=\int_{r_{ap}}^{r_h}\gamma_a(r,\bar{x})\ \mathrm{d}r=\dfrac{1}{G_a}\int_{r_{ap}}^{r_h}\tau(r,\bar{x})\ \mathrm{d}r\\ \Delta_p(\bar{x})=\int_{r_c}^{r_{ap}}\gamma_p(r,\bar{x})\ \mathrm{d}r=\dfrac{1}{G_a}\int_{r_c}^{r_{ap}}\tau(r,\bar{x})\ \mathrm{d}r\end{cases} \tag{13}$$

Substituting Eqs. (12) and (13) into Eq. (1), making use of Eqs. (6) and (7), differentiated two times about $\bar{x}$, and let

$${\lambda_1}^2=\frac{2}{E_c{r_c}^2\left[\dfrac{1}{G_a}\ln\dfrac{r_h}{r_{ap}}+\dfrac{1}{G_p}\ln\dfrac{r_{ap}}{r_c}\right]} \tag{14}$$

We can obtain

$$\frac{\partial{\tau_{ap}}^2\left(r_{ap},\bar{x}\right)}{\partial^2\bar{x}}-{\lambda_1}^2\tau_{ap}\left(r_{ap},\bar{x}\right)=0 \tag{15}$$

Considering Eqs. (5) and (10), noticing Eq. (7), when $r=r_h$, $\tau(r_h,\bar{x})=\dfrac{r_{ap}}{r_h}\tau_{ap}\left(r_{ap},\bar{x}\right)$, if let

$${\lambda_2}^2=\frac{\dfrac{2}{E_c{r_c}^2}+\dfrac{by}{E_hS_z^*r_h}}{\dfrac{1}{G_a}\ln\dfrac{r_h}{r_{ap}}+\dfrac{1}{G_p}\ln\dfrac{r_{ap}}{r_c}} \tag{16}$$

then we obtain

$$\frac{\partial{\tau_{ap}}^2\left(r_{ap},\bar{x}\right)}{\partial^2\bar{x}}-{\lambda_2}^2\tau_{ap}\left(r_{ap},\bar{x}\right)=0 \tag{17}$$

Let $\lambda=(\lambda_1,\ \lambda_2)$, consequently, Eqs. (15) and (17) can be unified as

$$\frac{\partial{\tau_{ap}}^2\left(r_{ap},\bar{x}\right)}{\partial^2\bar{x}}-\lambda^2\tau_{ap}\left(r_{ap},\bar{x}\right)=0 \tag{18}$$

2.3 Solutions to equations

The complete solution to Eq. (18) is given by

$$\tau_{ap}\left(r_{ap},\bar{x}\right)=A\cosh(\lambda\bar{x})+B\sinh(\lambda\bar{x}) \tag{19}$$

where A and B are integral constants decided by the boundary conditions. Considering Eq. (4), $\varepsilon_c(r_c, 0) = \varepsilon_h(r_h, 0)$ and when $\bar{x} = l_f$ the fibre-optic axial force is zero, then

$$N_c(0) = \sigma_h \pi r_c^2 \frac{E_c}{E_h}, \quad N_c(l_f) = 0 \tag{20}$$

where l_f is the distance measured from the mid-beam ($\bar{x} = 0$) to the point of zero axial load of the fibre. Using the above boundary condition, constants A and B are obtained by

$$A = \frac{\sigma_c r_c^2 \lambda}{2 r_{ap} \sinh(\lambda l_f)}, \qquad B = 0 \tag{21}$$

Combining Eqs. (21) and (19) yields the final form of the shear stress distribution between the adhesive layer and the protective coating

$$\tau_{ap}(r_{ap}, \bar{x}) = \frac{\sigma_c r_c^2 \lambda}{2 r_{ap} \sinh(\lambda l_f)} \cosh \lambda l_f \tag{22}$$

Further, the axial stress of the bare optic fibre $\sigma_c(\bar{x})$, can be determined by

$$\sigma_c(\bar{x}) = \sigma_c \left[1 - \frac{\sinh(\lambda \bar{x})}{\sinh(\lambda l_f)}\right] \tag{23}$$

Considering the compatibility condition (Eq. (11)), the axial strain, $\varepsilon_c(\bar{x})$, in the fibre core region is given by

$$\begin{cases} \varepsilon_c(\bar{x}) = \varepsilon_c(0)\left[1 - \dfrac{\sinh(\lambda \bar{x})}{\sinh(\lambda l_f)}\right] \\ \varepsilon_c(\bar{x}) = \varepsilon_h(0)\left[1 - \dfrac{\sinh(\lambda \bar{x})}{\sinh(\lambda l_f)}\right] \end{cases} \tag{24}$$

where $\varepsilon_h(0)$ is the axial strain of the host material at $\bar{x} = 0$.

From Eq. (24), it is clearly shown that the fibre-optic strain distribution along the axial direction is determined by the constant λ. This parameter is a function of the material properties, the geometric shape of the bare optical fibre, protective coating, adhesive layer, and host material (when the length of FGB sensor is not less). These properties and factors are the basic complications that affect the strain sensing rules. Conveniently these properties can be used to analyze the interface transferring mechanism of the FBG sensor.

2.4 General expression of multiplayer interface stain trasferring mechanism

Considering n-layer mediums between the optical fibre and the host material shown in Fig. 6, the analysis method and the solution format of the strain interface-transferring rule are completely the same. The only difference is in the eigenvalue λ. Based upon the above analysis, the eigenvalue λ can be written as the following unified expression

$$\begin{cases} \lambda_1^2 = \dfrac{2}{E_0 r_0^2 \sum\limits_{i=1}^{n}\left(\dfrac{1}{G_i} \cdot \dfrac{r_i}{r_{i-1}}\right)} \\ \lambda_2^2 = \dfrac{\dfrac{2}{E_0 r_0^2} + \dfrac{by}{E_h S_z^* r_n}}{\sum\limits_{i=1}^{n}\left(\dfrac{1}{G_i} \cdot \dfrac{r_i}{r_{i-1}}\right)} \end{cases} \tag{25}$$

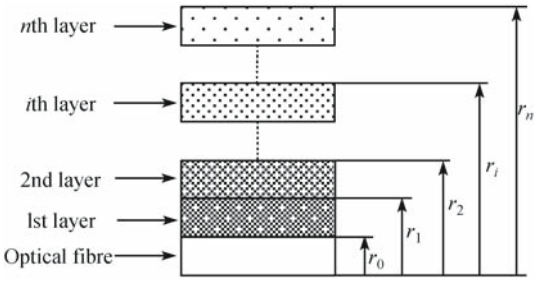

Fig. 6 Sketch of n-layer coating for optical fibre

The symbols r_0, E_0, r_i and G_i represent the outer radii and the elastic modulus of the optical fibre, and the outer radii and the shear modulus of the ith layer encapsulated material, respectively.

3 Average strain of the FBG sensor

From Eq. (24), it is clear that there is a difference at the testing point between the axial strain of the optical fibre ($\varepsilon_c(\bar{x})$) and the host material ($\varepsilon_h(0)$). If and only if $\bar{x} = 0$, then $\varepsilon_c(0) = \varepsilon_h(0)$. While monitoring, we can not obtain the strain of every $\bar{x}$ where the FBG sensor is set up. Hence, in order to estimate the error between the testing strain of the FBG sensor and the practical strain of the host material and modify it, the average measured strain of the FBG sensor and the host material are defined as

$$\bar{\varepsilon}_c = \frac{\int_0^{l_f} \varepsilon_c(\bar{x}) \mathrm{d}\bar{x}}{l_f}, \qquad \bar{\varepsilon}_h = \frac{\int_0^{l_f} \varepsilon_h(\bar{x}) \mathrm{d}\bar{x}}{l_f} \tag{26}$$

In addition, let $\bar{\varepsilon}_h = \varepsilon_h(0)$, noticing Eq. (24), then the relationship of average strains is

$$\bar{\varepsilon}_c = \bar{\varepsilon}_h \left(1 - \frac{\cosh(\lambda l_f) - 1}{\lambda l_f \sinh(\lambda l_f)}\right) \tag{27}$$

We define the error rate η and modified coefficient k as

$$\eta = \frac{|\bar{\varepsilon}_c - \bar{\varepsilon}_h|}{\bar{\varepsilon}_h} = \frac{\cosh(\lambda l_f) - 1}{\lambda l_f \sinh(\lambda l_f)} \tag{28}$$

$$k = \frac{1}{1-\eta} \tag{29}$$

then

$$\overline{\varepsilon}_{\mathrm{h}} = k\overline{\varepsilon}_{\mathrm{c}} \tag{30}$$

This equation gives the relationship between the FBG sensor testing strain and the practical strain of the host material, as well as affords the theory base for the analysis and modification of the system error.

4 Error analysis and modification

From the basic expressions Eqs. (42) and (43) of the FBG strain transfer, it is obvious that the FBG sensors have system errors, which are induced by the material properties and the geometry of the adhesive layer, protective coating and the bare optical fibre. Hence, it is a basic thing for us to accurately estimate the testing errors as well as efficiently modify them correctly, applying available FBG sensors and developing a new type of sensor. Following that, we will analyze and research the interface strain transferring errors and modification of the embedded tube-packaged FBG and FRP-OFBG sensors developed by us as well as give the influence on the interface strain transferring errors resulting from the geometric factors and the physical properties of the sensors and modify them.

4.1 Interface transfer and error modification of embedded tube-packaged FBG sensor

Figure 7 is the sketch map of the tube-packaged FBG sensor embedded in the structures.

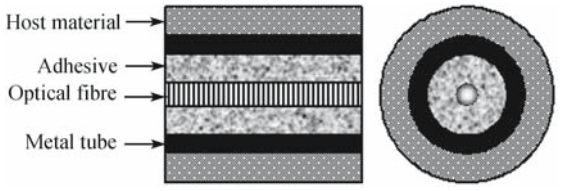

Fig. 7 Tube-encapsulated FBG embedded in structure

According to Eq. (25) and the conformation of the tube-packaged FBG sensor embedded in the structures, we can obtain λ as

$$\lambda^2 = \frac{2}{E_{\mathrm{c}} r_{\mathrm{c}}^2 \left[\frac{1}{G_{\mathrm{m}}} \ln \frac{r_{\mathrm{h}}}{r_{\mathrm{ma}}} + \frac{1}{G_{\mathrm{a}}} \ln \frac{r_{\mathrm{ma}}}{r_{\mathrm{c}}} \right]}, \; G_{\mathrm{m}} >> G_{\mathrm{a}} \tag{31}$$

where the symbols E_{c}, G_{m}, G_{a}, r_{ma}, r_{h} and r_{c} represent the elastic modulus of the FBG, the shear modulus of the metal tube and the adhesive layer, inner and outer radii of the metal tube and the outer radii of the fibre.

From Eq. (31), it is clear that because E_{c} and r_{c} are constants, the other variables, E_{c}, r_{c}, r_{ma} and r_{h}, are the main factors affecting the strain transferring errors. According to Eqs. (28) and (31), the function between the error rate η and the shear modulus is descending. Commonly, $G_{\mathrm{m}} >> G_{\mathrm{a}}$, from Eq. (31), the influence resulting from the metal tube (first item in the bracket) is much smaller than the one from the adhesive layer (second item in the bracket). Hence, while choosing the capillary metal tube, we especially research the influence on the strain transfer due to the shear modulus of the adhesive layers.

We chose the metal tube that has a shear modulus of 80 GPa and an outer radius of 1.2 mm as the encapsulation. The shear modulus of the adhesive changes from 20 to 1 000 MPa, inner radius (adhesive layer) respectively is 0.2 mm, 0.4 mm, 0.6 mm and 0.8 mm. Using Eq. (31), the numerical results of the error rate η caused by the shear modulus of the adhesive layers can be obtained and shown in Fig. 8, where $d_{\mathrm{ma}} = 2r_{\mathrm{ma}}$. Choosing an inner radius from 0.062 5–0.6 mm, the shear modulus of the adhesive layer are respectively 30, 50, 100, 300 and 1 000 MPa, then the results of error rate η induced from the inner radius of the metal tube are shown in Fig. 9.

From Figs. 8 and 9, the theoretical predictions reveal that the strain transfer error rate η of the tube-packaged FBG drops

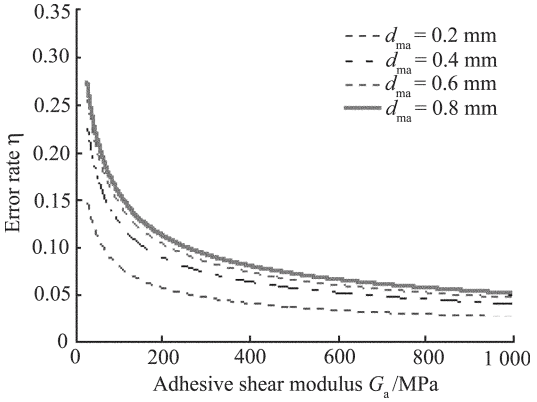

Fig. 8 Influence of adhesive shear modulus on strain transfer error rate

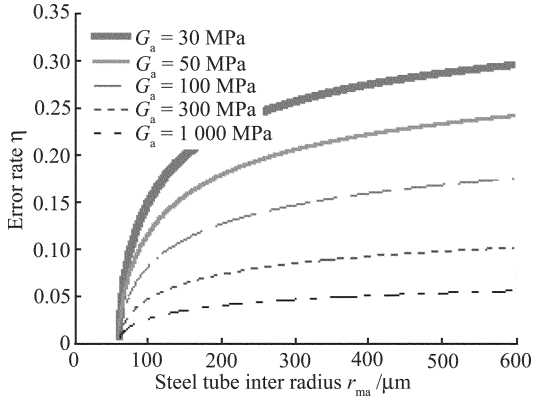

Fig. 9 Influence of tube radius on strain transfer error rate

against the shear modulus and rises against the thickness of the adhesive. For the shear modulus of the adhesive in 30–200 MPa and inner radius between 62.5 and 200 μm, the error rate is about 5%–10%, and as a result, the error modification must be considered in application. For the tube-packaged FBG we chose, the shear modulus of the adhesive is 39 MPa and an inner radius of 77.5 μm, the error rate $\eta = 9.92\%$ and the modification coefficient $k = 1.09\ 8$.

4.2 Strain transfer errors and modification of embedded FRP-OFBG

The sketch map of the FRP-OFBG embedded in the structure is shown in Fig. 10. As a strain sensor, usually the FRP-OFBG is shorter than the others, so the influence of the host materials can be ignored.

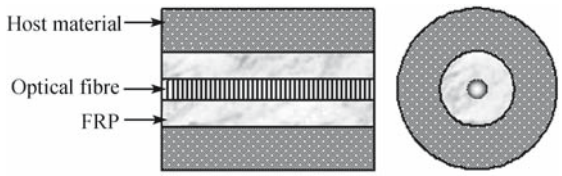

Fig. 10 FRP-OFBG embedded in structure

According to Eq. (25), taking $i = 1, E_0 = E_c, r_0 = r_c, r_1 = r_h$ and $G_1 = G_{FRP}$, then eigenvalue λ of FRP-OFBG can be expressed as

$$\lambda^2 = \frac{2G_{FRP}}{E_c r_c^2 \ln \frac{r_h}{r_c}} \tag{32}$$

Similarly, because E_c and r_c are constants, G_{FRP} and r_h are the main factors that affect the strain transferring errors.

Usually, the FRP-OFBG includes two kinds as GFRP-OFBG and CFRP-OFBG. For the GFRP-OFBG, the shear modulus of the GFRP changes from 3–9 GPa and the diameter of the GFRP bar is ϕ2–20 mm. If the elastic modulus, radius and length of FBG are $E_c = 70$ GPa, $r_c = 6.25 \times 10^{-2}$ mm, $l_f = 10$ mm respectively, substituted into Eq. (28), the relationship between the shear modulus of GFRP and the error rate can be obtained and shown in Fig. 11. Similarly, when the radius of the GFRP is 1–10 mm and the shear modulus is 10, 8, 4.9 and 3 GPa, the relationship of the radius and the error rate can be given and displayed in Fig. 12.

From Figs. 11 and 12, the theoretical predictions imply that the strain transfer error rate η of the GFRP reduces against the shear modulus and increases against the radius. For the shear modulus of the GFRP in 4–9 GPa and the diameter between 6 and 12 mm, the error rate is less than 4%. Considering the GFRP-OFBG smart composite bar developed by ourselves, the shear modulus is 4.9 GPa, and the diameter is ϕ4, ϕ6, and ϕ10 mm respectively, and correspondingly, the error rate η is 3.11%, 3.29% and 3.5% while the error modification coefficient k is 1.032, 1.034 and 1.036. Using

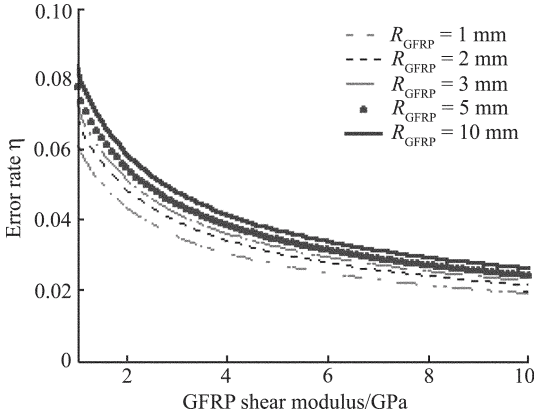

Fig. 11 Influence of GFRP shear modulus on strain transfer error rate

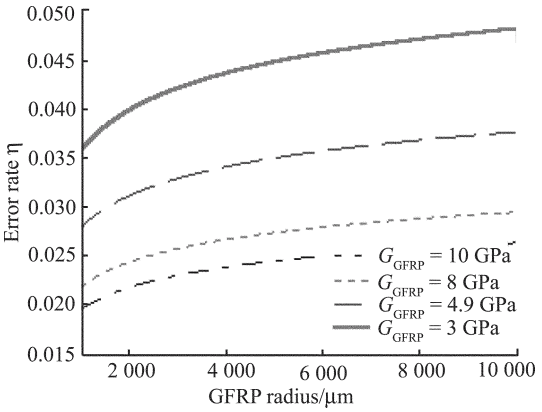

Fig. 12 Influence of GFRP radius on strain transfer error rate

the same analysis, we can find that the CFRP-OFBG'S error rate is less than 2.5% under a radius of 1–10 mm and the shear modulus is 30, 20, 15 and 12.8 GPa, shown in Figs. 13 and 14.

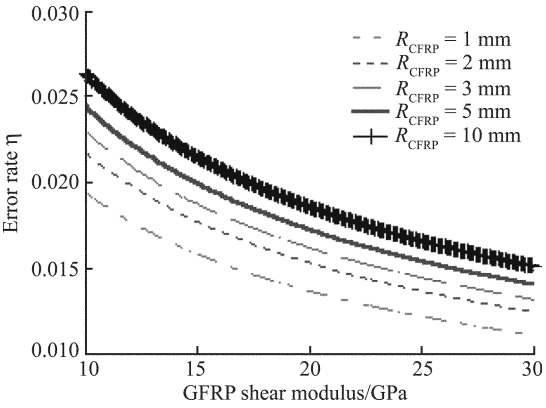

Fig. 13 Influence of CFRP shear modulus on strain transfer error rate

In a word, whether it is the GFRP-OFBG or the CFRP-OFBG, the error rate is less than 3.5%, and especially the CFRP is less than 2.5%. The main reason is that the shear modulus of CFRP is large. Because an error rate of 3.5% is allowed in application, the FRP-OFBG bars are not to be modified and the testing strain is thought to be precise.

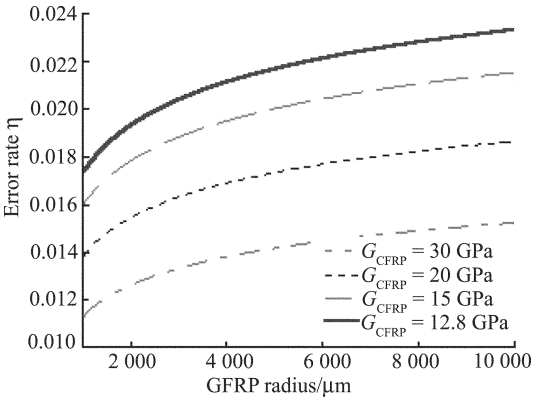

Fig. 14 Influence of CFRP on strain transfer error rate

5 Example of error analysis and modification for FBG sensors

According to the above, owing to the low error rate of FRP-OFBG (less than 3.5%), which meets the precision requirement, the strain it measures is exact and need not be modified. Moreover, the error rate of the embedded tube-packaged FBG sensors is between 5% and 10%, so it must be modified in application.

In order to explain the correctness of the above theories as well as validating the results of modifying the FBG error rate, we find that there is an obvious difference in testing strains between the GFRP-OFBG and FBG sensors put into the same location of FRP concrete beam. However, the strain tested by the FBG coincides very well with the GFRP-OFBG after being modified by the above method. Not only is the correctness of the theory analysis proved, but also the necessity of the error modification to the FBG sensors is explained. The result is shown in Fig. 15.

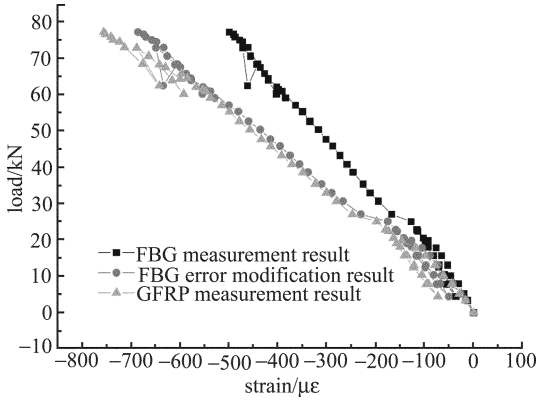

Fig. 15 Comparison between the results from error modification and the original

6 Conclusions

This paper studies an embedded FBG sensor. The general expression of a multilayer interface strain transferring mechanism was derived. Then, based on the defined average strain, the error modified equation of the FBG sensor was obtained. Finally, in the light of the embedded tube-packaged FBG and the FRP-OFBG strain sensors that we developed, the corresponding strain transferring error and laws were studied, and the corresponding error modification coefficients were given too, which were validated by experiments. Research indicated the following.

First, the interface transfer error of the fibre-optic sensors must be considered in an application.

Second, for CFRP-FBG smart composite bars whose shear modulus is more than 12 GPa and the outer diameter is $\phi 4$–$\phi 10$ mm, the error rate is between 1.92% and 2.16%, and the modification coefficient is 1.02–1.022. Moreover, towards GFRP-FBG smart composite bars, when the shear modulus is larger than 4.9 GPa and the diameter changes from $\phi 4$ mm to $\phi 10$ mm, the error rate is 3.11%–3.5% and the modification coefficient between 1.034 and 1.036. So they need not to be modified.

Third, according to the tube-packaged FBG sensors, when the shear modulus of the adhesive ranges into 30–200 GPa and the outer diameter is less than 200 μm, the error rate is about 5%–10%, and it must be modified and the corresponding modification coefficient is 1.05–1.1.

Acknowledgements This work was supported by the National Natural Science Foundation of China (Grant Nos. 50308008, 10672048, 50278029) and the China Postdoctoral Science Foundation.

References

1. Nanni A, Yang C C, Pan K, et al. Fiber-optic sensors for concrete strain/stress measurement. ACI materials Journal, 1991, 88(3): 257–264
2. Ansari F, Yuan L. Mechanics of bond and interface shear transfer in optical fibre sensors. J Eng Mech 1998, 124(4): 385–394
3. Duck G., Renaund G., Measures M. The mechanical load transfer into a distributed optical fibre sensor due to a linear strain gradient: Embedded and surface bonded case. J Smart Mater Struct, 1999, 8: 175–181
4. Lau Kintak, Yuan Libo, Zhou Limin, et al. Strain monitoring in FRP laminates and concrete beams using FBG sensors. Composite Structures, 2001, 51: 9–20
5. Zhou Zhi, Wu Zhanjun, Ou Jinping. Technique and application of in-situ monitoring for concrete structures with FBG sensors. Pacific Science Review, Far East Technical University of Russian, Vlasivostok, 2002 (in Chinese)
6. Ou Jinping, Zhou Zhi, Wu Zhanjun. The sensing properties and practical application in civil infrastructures of optical FBGs. SPIE, 2003 (in Chinese)
7. Zhou Zhi, Zhao Xuefeng, Ou Jinping, et al. A coating technique with steel capillary for FBG and its sensing properties. Chinese Laser, 2002, 29(12): 1089–1092 (in Chinese)
8. Zhou Zhi, Wu Zhanjun, Ou Jinping, et al. Smart monitoring technique of concrete structures based on optical fiber bragg grating sensors. Function Materials, 2003, 34(3): 344–348 (in Chinese)
9. Zhou Zhi. Optical fiber smart bragg grating sensors and intelligent monitoring systems of civil infrastructures. Ph. D. Dissertation. Harbin: Harbin Institute of Tech., 2003: 33–34
10. Triantafillou T C. Shear strengthening of reinforced concrete beams using epoxy-bonded FRP composites. J ACI Struct, 1998, 95(2): 107–115